Original Research Article

Novel Graphitic Carbon Nitride/Co-B-PNanocomposites with Significantly EnhanceVisible-Light Photocatalytic HydrogenProduction from Water Splitting

ABSTRACT

As a promising metal-free photocatalyst for hydrogen (H_2) production through water splitting under visible-light irradiation, graphitic carbon nitride (g-C_3N_4) photocatalysts decorated with CoBP were prepared via simple ultrasonification. This paper highlights the structures of the photocatalysts, their stability, rate of hydrogen evolution and the mechanism of charge transfer within the photocatalysts. The prepared C_3N_4/CoBP nanocomposite photocatalysts were characterised by using X-ray diffraction, X-ray photoelectron spectroscopy, transmission electron microscopy, scanning electron microscopy and UV–visible (UV–vis) diffuse reflectance spectroscopy. After detailed analysis, the C_3N_4/CoBP nanocomposite photocatalysts showed excellent photocatalytic performance, which was due to the formation of the heterostructured hybrids of g-C_3N_4 and CoBP. The effects of C_3N_4/CoBP nanohybrids on H_2 evolution were evaluated. The effects improved with increasing load of CoBP until the optimal level (5 wt% CoBP with visible-light irradiation at λ ≥420 nm). The maximum and remarkable photocatalytic H_2 evolution rate of 51.68 μmol h^{-1} was achieved, which was 3.8 times that obtained from pure g-C_3N_4. Moreover, the C_3N_4/CoBPheterostructured nanohybrids demonstrated extremely high photostability and recyclability for H_2 evolution after visible light illumination. The composite hybrid accelerated the separation and transfer of photogenerated charge carriers and subsequently suppressed charge recombination. Conclusively, this study offered an opportunity for the design and synthesis of highly stable and efficient C_3N_4/CoBP nanocomposite photocatalysts for energy conversion and utilisation.

Keywords: Heterostructured photocatalyst, C_3N_4/CoBP nanocomposite, water splitting, hydrogen evolution, charge separation efficiency.

1. INTRODUCTION

Hydrogen (H_2) is considered as a clean, renewable, environmental friendly and attractive alternative energy source compared with fossil fuels[1,2]. After Fujishima and Honda reported photoelectrochemical water splitting over a TiO_2 electrode in 1972[3], photocatalyticH_2 production via water splitting under solar irradiation has become the most fascinating and promising strategies for solving the energy crisis and environmental pollution[4–6]. In the past few years, extensive effort has been devoted to designing and developing various semiconductor-based photocatalysts for H_2 production via water splitting. It includes but not limited to oxides[7], sulphides[8], nitrides[9] and conjugated polymer[10,11]. However, most of these materials are limited for practical requirements because of low efficiency, poor chemical stability and high costs[4,5,10]. Therefore, to improve the efficiency of photocatalytic H_2 production through water splitting, considerable attention has been paid to developing potential semiconductor photocatalysts with high efficiency, chemical stability and response to visible-light irradiation.

Recently, graphitic carbon nitride (g-C_3N_4), has emerged as a typical metal-free organic semiconductor photocatalyst for visible light photocatalytic H_2 production via water splitting. Since 2009[12], g-C_3N_4 photocatalyst associated with the

unique properties of g-C_3N_4,such as appropriate band gap (~2.7 eV), excellent in physical and chemical stability, abundance and non-toxicity, have been extensively studied[13,14]. However, the photocatalytic performance of the H_2 evolution of pristine g-C_3N_4 seems to be limited because of its poor light absorption and the fast recombination rate of photo induced charge carriers[15]. To overcome these problems, researchers have developed different strategies that improve the photocatalytic efficiency of pure g-C_3N_4, such as doping with metal or non-metal elements[1,14], controlling morphology[16,17] and constructing heterojunctions with other semiconductors[5,7,13].

Constructing heterojunctions between g-C_3N_4 photocatalysts and other materials has been identified as the most effective and feasible route for the improvement of charge migration and separation in g-C_3N_4[5,7,13]. Therefore, g-C_3N_4 can be merged with a suitable material to form a g-C_3N_4-based heterostructure photocatalyst for H_2 production. Various cobalt-based compounds, such as CoO[18], Co_3N[19] and $Co(OH)_2$[20] are widely used as effective catalysts for constructing g-C_3N_4-based composite photocatalysts and show outstanding performance in photocatalytic H_2 evolution reactions. Ternary cobalt-based catalyst (CoBP) has been found to intensify significant attention in the electrocatalysis studies of H_2 production enhanced by its synergistic effect of elements P and B[21–23]. For example, Hongming Sun *et al*.[21] synthesized CoBP nanosheets supported on a Ni foam; the nanosheets were showed remarkably enhanced electrocatalytic activity in H_2 evolution. Chunduri *et al*.[22]synthesized an amorphous CoBP bifunctional electrocatalyst to enhance alkaline water splitting in electrocatalytic H_2 production reaction. Thus, a more efficient g-C_3N_4-composite can be designed according to CoBP catalyst to enhance the photocatalytic performance of H_2 production. However, the synthesis of C_3N_4/CoBP nanocomposite photocatalyst for photocatalytic H_2 production through water splitting under visible-light irradiation has not been reported.

The present study is the first to report a novel C_3N_4/CoBP nanocomposite photocatalyst by decorating an amorphous CoBP on the surface of a g-C_3N_4 photocatalyst via a simple ultrasonic process. The obtained C_3N_4/CoBP nanocomposite photocatalyst showed higher photocatalytic activity and stability for H_2 evolution under visible-light irradiation than pure g-C_3N_4. The maximum H_2 evolution rate was obtained after 5 wt% amorphous CoBP was loaded on the surface of g-C_3N_4 and reached a rate of 51.68 μmol h^{-1}, which was 3.8 times that of pure g-C_3N_4. The heterojunction formed between the planar aromatic structure g-C_3N_4 and CoBP molecule accelerated interfacial charge migration and separation. Consequently, the C_3N_4/CoBP nanocomposite photocatalyst exhibited significantly high photocatalytic activity for H_2 production. Therefore, merging CoBP with g-C_3N_4 is a promising method for developing efficient and low-cost photocatalysts for H_2 production through water splitting. This work can provide novel insights into the planning, design and development of efficient photocatalysts with high activity for solar energy applications.

2. MATERIAL AND METHODS

2.1 Chemicals.

Urea (≥ 99 %), cobalt (II) chloride hexahydrate ($CoCl_2.6H_2O$), ammonium chloride (NH_4Cl), ammonia solution, sodium hypophosphite monohydrate ($NaH_2PO_2.H_2O$), sodium hydroxide (NaOH), anhydrous sodium sulfate (Na_2SO_4), triethanolamine (TEOA, ≥ 78 %), methanol (≥ 99%), lactic acid (≥ 85%) and ascorbic acid (≥ 99%) were purchased from Sinopharm Chemical Reagent Co., Ltd. sodium borohydride ($NaBH_4$) and Chloroplatinic acid hexahydrate ($H_2PtCl_6.6H_2O$, ≥ 37 % Pt basis) were bought from Aldrich. All chemicals were of analytical grade and used as received from the manufactures without any purification. Double distilled water was produced from a SZ-93A auto-double distillation apparatus (Ya Rong Corp., Shanghai, China).

2.2 Preparation of the photocatalyst.

2.2.1 Preparation of g-C_3N_4

Firstly, 10.0 g of urea was added into covered alumina crucible and calcined at 550 °C for 4 h in a muffle furnace under air atmosphere, at the heating rate of 5 °C min^{-1}. After 4 h, the sample was left to cool naturally to room temperature, yellow powder (g-C_3N_4) was obtained was collected for further use.

2.2.2 Preparation of Amorphous CoBP

CoBP was prepared by a modified an electroless deposition method[21]. In a typical synthesis, solution A containing a 50 mL of aqueous solution of $CoCl_2.6H_2O$ (3.5 mmol), NH_4Cl (25 mmol) and some amount of $NH_3.H_2O$ (for adjusting pH to 9), was deaerated and flushed with argon. Meanwhile, a solution B containing a 50 mL of aqueous solution of $NaBH_4$ (35 mmol), $NaH_2PO_2.H_2O$ (500 mmol) and NaOH (3.8 mmol) which was also deaerated and flushed with argon. Then, solution B was added drop wise to solution A under ultrasonification in an ice bath (ultrasonification was applied throughout the reaction process). Vigorous frothing occurred and a dark product was formed. After the completion of the reaction, the sample was centrifuged and washed thoroughly with distilled water and dried at 50 °C under vacuum, and the corresponding sample was labelled Co-B-P.

2.2.3 Preparation of g-C_3N_4/CoBP composite photocatalyst

The C_3N_4/CoBP composite photocatalyst was obtained by mixing an appropriate amount of g-C_3N_4 and CoBP in solution and then was placed in ultrasonic bath for 3 h, followed by drying for the removal of solvent.

2.3 Characterization.

The crystal phase of the samples were characterized by powder X-ray diffraction (XRD) measurements using X-ray diffractometer (MXPAHF, Japan) with Cu Kα irradiation (λ = 1.541 Å) at operating voltage of 40 kV and a current of 200 mA. Morphology of the photocatalysts was confirmed by Transmission electron microscopy (TEM) on JEOL-2010, Japan) at accelerating voltage of 200 kV. The XPS was recorded to study the elemental composition and binding energies of the sample and operated by ESCALAB 250 high-performance electron spectrometer which was set to monochromated Al Kα radiation as the excitation source. The UV-vis diffuse reflectance spectra of the photocatalysts were recorded by a Shimadzu spectrophotometer (Model 2501 PC). The steady-state photoluminescence (PL) specra were conducted on a fluorescence spectrophotometer (JY Fluorolog-3-Tau) with the excitation wavelength at 325 nm. The time-resolved photoluminescence (TRPL) was measured on a Laser Strobe Time-Resolved Spectrofluorometer (Photon Technology International (Canada) Inc.) with a USHIO xenon lamp source, a GL-302 high-resolution dye laser (lifetimes 100 ps to 50 ms, excited by a Nitrogen laser) and a 914 photomultiplier detection system.

2.4 Photoelectrochemical measurements

Photoelectrochemical tests were carried out at CHI 760E electrochemical workstation (Chenhua Instrument Company, Shanghai, China) based on a standard three-electrode system, composed of Ag/AgCl as the reference electrode, Pt wire as the counter electrode and indium-tin oxide (ITO) glass as the working electrode. Na_2SO_4 (0.5 M) was used as the electrolyte solution. A 300 W Xe lamp was used as a solar light source (λ ≥ 420 nm). For the preparation of working electrodes, 2 mg of either g-C_3N_4 or C_3N_4/5 wt% CoBP samples was dispersed in 1 mL ethanol and 10 µL Nafion solution by ultrasonification process. The resulting dispersion was spin-coated onto a piece of ITO glass with a fixed area of ca. 1 cm^2 and annealed at 300 °C for 2 h to remove the organic species completely. The amperometric photocurrents were measured for each switch on/off event with a bias voltage of 0.5 V under visible light irradiation. The electrochemical impedance spectroscopy (EIS) was recorded under visible light and a bias of −1 V and the frequency range was from 10 mHz to 100 kHz in parallel to an alternating current signal amplitude of 5 mV.

2.5 Photocatalytic hydrogen production test.

The photocatalytic hydrogen evolution from water splitting was carried out in an outer Pyrex top-irradiation reaction vessel (500 mL) connected to a glass closed gas circulation system. In a typical experiment, 10 mL of triethanolamine (TEOA) was used as a sacrificial agent in an aqueous solution of 100 mL. 50 mg of g-C_3N_4 powder and CoBP with different amounts were dispersed in water and then kept in an ultrasonic bath for half an hour. And 1 wt% Pt， as a co-catalyst to boost H_2 generation was loaded onto the surface of the catalyst by in situ photodeposition method using $H_2PtCl_6.6H_2O$. In order to make sure anaerobic conditions in the reaction system, the solution was evacuated 1 h to remove air completely before irradiation by a 300 W xenon lamp (Perfect Light, PLS-SXE300C, Beijing). The xenon lamp is equipped with a cut-off filter (λ ≥ 420 nm) to remove ultraviolet light. Besides, the Pyrex reactor with a double layer was continuously stirred, and a flow of cooling ethylene glycol was used during the photocatalytic reaction to maintain the temperature of the reaction solution at 10 °C. The amount of hydrogen evolution from photocatalytic splitting water was measured using on-line gas chromatography (GC1120, Shanghai Sunny Hengping Limited, HTCD, nitrogen as carrier gas). After the reaction, the photocatalysts were separated from the reaction solution for further characterization. The catalysts are denoted as C_3N_4/x CoBP, where x (x = 4, 5, 6 %) refers to the weight content of CoBP in C_3N_4/CoBP samples.

The apparent quantum yield (AQY) was measured under different monochromatic light irradiation by using C_3N_4/5 wt% CoBP photocatalyst (irradiated by a 300 W Xe lamp using the bandpass filter of λ ± 5 nm for 420, 450, 500, 550, 600 nm), and was calculated according to the equation given below:

$$\text{AQY (\%)} = \frac{\text{Number of reacted electrons}}{\text{Number of incident photons}} \times 100\%$$

$$= \frac{\text{Number of evolved } H_2 \text{ molecules} \times 2}{\text{Number of incident photons}} \times 100\%$$

3. RESULTS AND DISCUSSION

Graphitic carbon nitride (g-C_3N_4) was prepared from urea and calcined at 550 ^oC for 4 h, CoBP molecule was synthesised by an electroless deposition method (Fig. S1) and g-C_3N_4/CoBP nanocomposite photocatalysts were obtained by mixing g-C_3N_4 and CoBP in a solution and then dried. The X-ray diffraction (XRD) patterns of the samples prepared are displayed in Fig. 1a. Pure g-C_3N_4 exhibited two main diffraction peaks with different intensities. The low-angle diffraction peak at 13.0° index was attributed to the (100) plane, and the high-angle diffraction peak at 27.7° was attributed to the (002) lattice plane. These arrangements reflected an in-plane structural packing motif of a tri-s-triazine unit and the interlayer

stacking peak of conjugated aromatic systems observed for g-C_3N_4, respectively[6,24]. The XRD patterns of composite C_3N_4/CoBP with 5 wt% CoBP displayed similar diffraction peaks observed on the original g-C_3N_4. Remarkably, no other impurity phase was observed. The well-crystal structure of g-C_3N_4 was not affected by CoBP loading. In addition, no intense diffraction peaks were observed in the XRD pattern of pure CoBP confirming noncrystallinity, and only a single broad peak was detected (at approximately 45°; Fig. 1b), indicating the amorphous structure of CoBP[21,25,26]. In addition, EDS measurement of CoBP molecule was performed and the spectrum (Fig. S2) confirmed the existence of only Co, B, and P in the molecule.

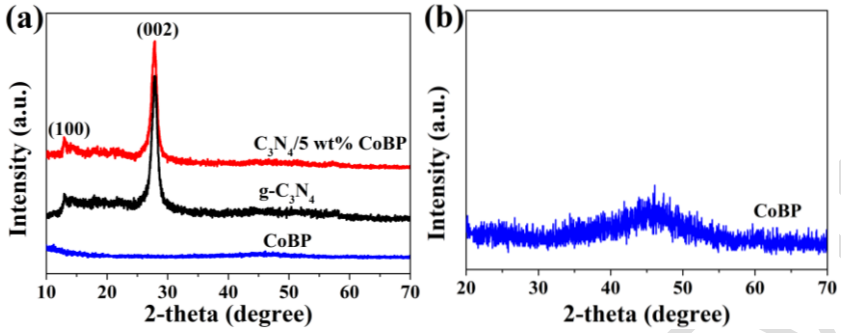

Fig.1. (a)XRD patterns of CoBP molecule, g-C_3N_4 and C_3N_4/5 wt% CoBP photocatalysts. (b) XRD patterns of amorphous CoBP.

The prepared CoBP molecule displayed a nanosphere morphology (Fig. 2a). However, after 5 wt% CoBP was loaded, the morphology of the composite photocatalyst C_3N_4/CoBP remained unchanged in contrast to the morphology of g-C_3N_4. This result demonstrated that CoBP did not affect the morphology of the g-C_3N_4 photocatalyst (Fig. 2b and c). The high-resolution TEM and selected area electron diffraction (SAED) images of CoBP were used in verifying the amorphous nature of CoBP. The HR-TEM image did not indicate the presence of any crystalline phase or lattice plane (Fig. 2d). This result was confirmed by the occurrence of diffused rings in the SAED image (inset of Fig. 2d)[21–23].

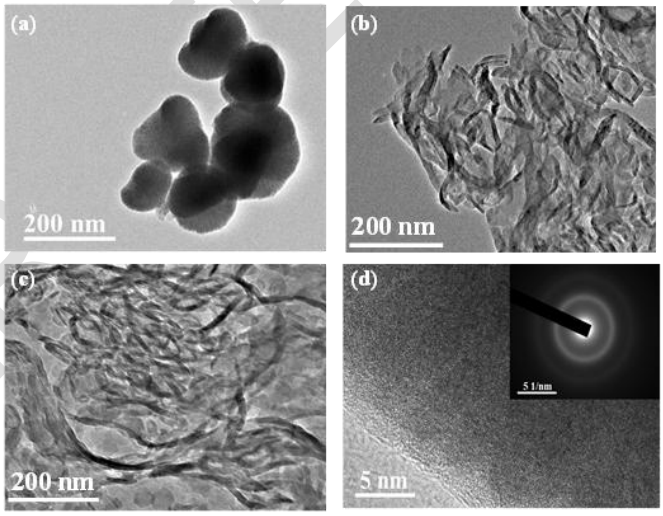

Fig.2. TEM images of (a) CoBP sample, (b) Pure g-C_3N_4, (c) g-C_3N_4/5 wt% CoBP photocatalysts. (d) HR-TEM image and SAED pattern (inset) of CoBP sample.

To investigate the chemical states of the prepared CoBP catalyst, an X-ray photoelectron spectroscopy (XPS) test was carried out (Fig. S3). The XPS spectrum of the Co 2p (Fig. S3a) displayed two major peaks. A strong peak was detected at a binding energy 780.7 eV for Co $2p_{3/2}$, and a minor peak at 796.5 eV for Co $2p_{1/2}$. In addition, two satellite peaks were detected in the Co 2p spectra at binding energy of 786.5 and 802.96 eV, confirming the presence of elemental Co and the oxidised state of Co in the catalyst[21–23,27]. The peaks of boron 1s were detected in the high-resolution XPS spectrum at 188.0 and 190.33 eV, which were attributed to boron in elemental and oxidised states, respectively (Fig. S3b). The binding energy of elemental boron shifted positively by 0.8 eV compared with the reported binding energy of pure boron (187.2 eV)[21,27]. With respect to P 2p high-resolution XPS spectrum (Fig. S3c),

phosphorous showed two distinct peaks at 129.5 and 132.83 eV, which might be assigned to the presence of P^o and oxidised phosphorous species, respectively[21–23,27].

In general, the photocatalytic activity of H_2 production through water splitting depended on the optical absorption efficiency of catalysts and can be employed to determine the band gap of semiconductor photocatalystd. The UV–visible (UV–vis) diffuse reflectance spectra of CoBP, g-C_3N_4 and C_3N_4/5 wt% CoBP composite photocatalyst were collected to show their optical properties. As shown in Fig. 3a, bare g-C_3N_4 absorbed visible light with absorption edge of approximately 450 nm (band gap of ~2.7 eV) because of the excitation of electrons from the valence band to the conduction band[28]. After 5 wt% CoBP was loaded, the composite C_3N_4/CoBP showed an absorption edge nearly similar to that of pure g-C_3N_4, confirming that no structural change occurred in g-C_3N_4. Additionally, the absorption intensity of g-C_3N_4 slightly increased after the loading of 5 wt% CoBP, showing that CoBP was successfully introduced to the surface of g-C_3N_4. Based on the UV-vis spectra, the optical band gap value of CoBP was calculated from the Kubelka–Munk method (Fig. 3b) and determined to be approximately 1.59 eV.

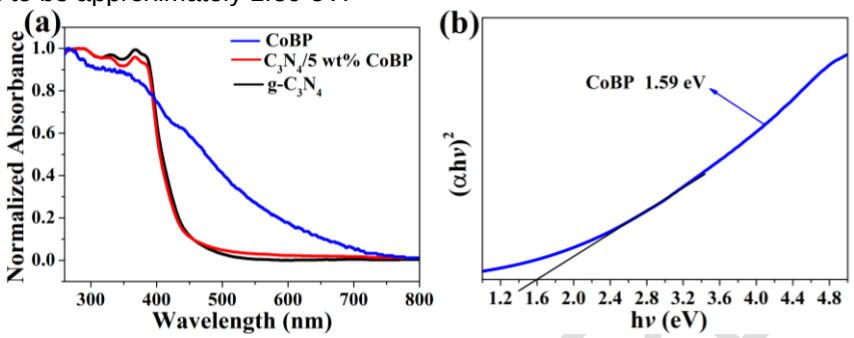

Fig. 3. (a)The diffuse reflectance UV-vis absorption spectra of solid CoBP molecule, g-C_3N_4 and C_3N_4/5 wt% CoBP photocatalysts. (b) Band gap evaluation from the plots of $(\alpha h\nu)^{1/2}$ vs the energy of the absorbed light of the NPBIm molecule.

To explore the migration, the transfer and separation of the photogenerated electron–hole pairs over g-C_3N_4 and C_3N_4/5 wt% CoBP samples, the steady-state photoluminescence (PL) and time-resolved photoluminescence (TRPL) spectra were recorded. As displayed in Fig. 4a, the PL emission peak of pure g-C_3N_4 centered at approximately 450 nm under an excitation wavelength of 325 nm at room temperature, resulting from the electron–hole recombination in g-C_3N_4[6,29]. The C_3N_4/5 wt% CoBP composite displayed an emission peak similar to that of pure g-C_3N_4, but the peak intensity significantly declined because of the effective suppression of photogenerated charge carriers. Thus, photocatalytic activity for H_2 production was boosted. The charge transfer efficiency within the composite was measured, and the results are shown in Fig. 4b. The average lifetimes of the photogenerated charge carriers for g-C_3N_4 and C_3N_4/5 wt% CoBP samples were 2.54 ± 0.21 and 3.11 ± 0.26 ns, respectively. Long lifetimes are ascribed to the rapid transfer and separation of photogenerated charge carriers and subsequent inhibition of recombination[6,24]. This result confirmed that loading a suitable amount of CoBP induces charge transfer and thereby significantly increase H_2 production rate.

Moreover, photoelectrochemical tests over g-C_3N_4 and C_3N_4/5 wt% CoBP samples were performed under visible-light irradiation (λ ≥ 420 nm) to investigate the effect of CoBP on the generation and migration of photogenerated charge carriers. As shown in Fig. 4c, under several on–off visible-light irradiation cycles of a photocurrent response, both electrodes generated rapid and constant photocurrent responses. Compared with the pure g-C_3N_4 photocatalyst, C_3N_4/5 wt% CoBP composite photocatalyst showed stable and higher photocurrent density (nearly twofold that of pure g-C_3N_4). The high photocurrent responses of C_3N_4/5 wt% CoBP hybrid indicated efficient charge migration and separation between g-C_3N_4 and CoBP interfaces[5,19]. This observation is a good indicator of the inhibited recombination of photogenerated electron and holes. This effect was in a good agreement with the results of PL spectra. In addition, the electrochemical impedance spectroscopy (EIS) test of g-C_3N_4 and C_3N_4/5 wt% CoBP was performed at an alternating current voltage of 0.5 V to study charge transfer resistance. As displayed in Fig. 4d, the C_3N_4/5 wt% CoBP sample exhibited a smaller arc radius than pure g-C_3N_4, implying efficient charge migration and separation, both of which are beneficial for the photocatalytic performance of H_2 production[19,30]. The obtained Nyquist plots data were fitted with the Randles circuit (Fig. 4d inset, where Rs and Rct represent solution resistance and charge transfer resistance between the electrolyte and electrode, respectively). The EIS-fitted parameters are displayed in Table S1 in Supporting Information. The results of photoelectrochemical tests showed that charge migration and separation indeed occurred at the interface between g-C_3N_4 and CoBP.

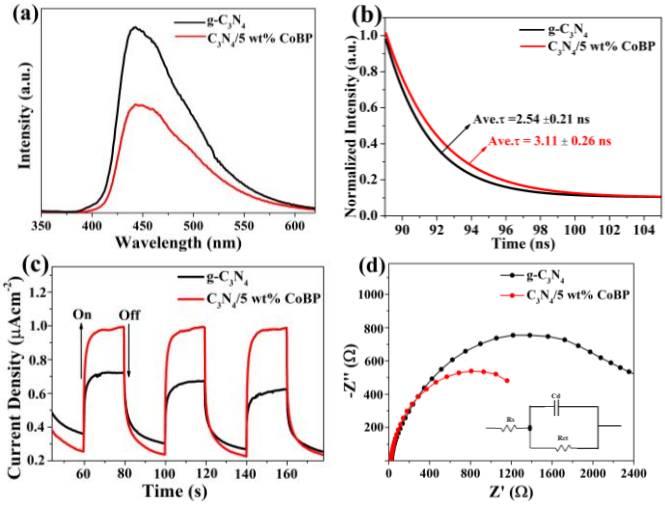

Fig. 4. (a)Steady-state photoluminescence spectra. (b) Time-resolved fluorescence decay traces for g-C_3N_4 and C_3N_4/5 wt% CoBP photocatalyst (excitation at 325 nm, emission at 450 nm). (c) Transient photocurrent response. (d) EIS Nyquist plots for g- C_3N_4 and C_3N_4/5 wt% CoBP under visible light irradiation (λ ≥ 420 nm, [Na_2SO_4] = 0.5 M). The inset correspond to the fitting using the equivalent circuit.

To compare the photocatalytic activity of H_2 evolution over different prepared photocatalysts, a series of comparative experiments were performed. Firstly, the H_2 evolution rate was measured by using different sacrificial agents under visible-light irradiation (λ ≥ 420 nm). As shown in Fig. S4, the C_3N_4/5 wt% CoBP composite photocatalyst exhibited a high H_2 evolution rate when triethanolamine (TEOA) was used as the sacrificial agent in the photocatalytic reaction. TEOA is suitable at high H_2 level because of its high redox potential and the created basic environment[31].Thus TEOA was considered the best sacrificial agent.

Furthermore, the H_2 evolution rate over different samples were measured under visible-light irradiation (Fig. 5). The sample of g-C_3N_4 with 1 wt% Pt cocatalyst (Fig. 5b) displayed high photocatalytic activity (13.47 μmol h^{-1}) compared with pure g-C_3N_4 (Fig. 5a) due to the fast recombination rate of photogenerated electron–hole pairs. The visible photocatalytic H_2 evolution rate of g-C_3N_4 significantly increased up to 51.68 μmol h^{-1} when 5 wt% CoBP was added (Fig. 5c). This value was 3.8 times that of pure g-C_3N_4. To confirm the role of CoBP in the photocatalytic system, the H_2 evolution rate of C_3N_4/5 wt% CoBP without deposition of Pt cocatalyst was 5.31 μmol h^{-1} (Fig. 5d). A controlled experiment was then performed for a pure CoBP sample. The results demonstrated that no hydrogen evolution occurred when only pure CoBP was used as the photocatalyst. These results showed that enhanced photocatalytic activity can be attributed to the formation of heterojunction in the C_3N_4/CoBP composite photocatalyst. The heterojunction facilitated charge transfer and separation, which in turn improved photocatalytic activity during H_2 evolution.

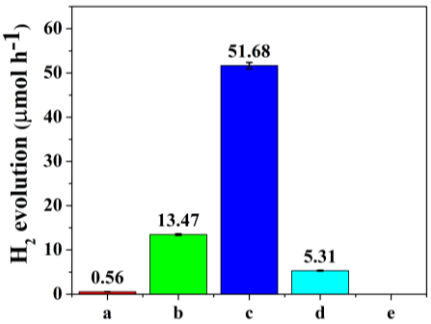

Fig. 5. Comparison of H_2 evolution rates over different samples; (a) g-C_3N_4 without the Pt cocatalyst, (b) g-C_3N_4 with 1% Pt, (c) C_3N_4/5 wt% CoBP with 1% Pt cocatalyst, (d) C_3N_4/5 wt% CoBP without the Pt cocatalyst, (e) CoBP alone without Pt cocatalyst: Reaction conditions: 50 mg of photocatalyst, λ ≥ 420 nm, 100 mL of solvent, H_2O/TEOA = 9:1 (vol/vol), light source, xenon lamp (300 W) with a cutoff filter; temperature, 10 °C.

Moreover, the photocatalytic H_2 evolution rates of g-C_3N_4 at different amounts of CoBP (4, 5 and 6 wt%) were further investigated under visible-light irradiation (λ ≥ 420 nm). TEOA was used as the sacrificial reagent (Fig. 6a). The introduction of CoBP greatly improved photocatalytic H_2 evolution rate. Pure g-C_3N_4 exhibited the extremely low photocatalytic activity of H_2 evolution rate (13.47 μmol h^{-1}). When 4 wt% CoBP was introduced, the H_2 evolution rate increased up to 36.37 μmol h^{-1}. Remarkably, when 5 wt% CoBP was loaded, the H_2 evolution rate further increased and reached a maximum value of 51.68 μmol h^{-1}, which was 3.8 that of bare g-C_3N_4. This value was higher than the maximum

values of other g-C_3N_4-based heterostructure photocatalysts (Table S2)[6,18,32,33]. As CoBP loading further increased to 6 wt%, the H_2 evolution rate decreased to 39.77 μmol h^{-1}. The possible reasons were as follows: (i) the black color of CoBP led to a significant increase in opacity and shielding effect that prevented incident light from reaching the surface of the g-C_3N_4 photocatalyst and (ii) an excessive amount of CoBP blocked active sites on the surface of g-C_3N_4 and impeded contact between the reactive sites and reactants[6,14]. Thus, loading a suitable amount of CoBP onto g-C_3N_4 is a suitable method for increasing photocatalytic activity in the H_2 evolution of C_3N_4/CoBP composite photocatalysts.

To test the reciprocal effects of Pt loading amount, we measured the activity of C_3N_4/5 wt% CoBP catalysts with varied wt% Pt loading content (Fig. S5). The surface area of a catalyst plays a vital role in the enhancement of photocatalytic activity of a catalyst. Catalysts with large specific surface areas have numerous active sites that improve light absorption[34]. Nitrogen sorption isotherms were measured to determine the specific surface areas of the prepared catalysts. As shown in Fig. S6, the BET specific surface areas (S_{BET}) of pure g-C_3N_4 and C_3N_4/5 wt% CoBP composite were 89 and 114 m^2g^{-1}, respectively. The composite photocatalyst showed higher S_{BET} than pure g-C_3N_4 because of the insertion of CoBP, and the addition of CoBP increased the surface area of the composite catalyst. This effect enhanced the performance of C_3N_4/5 wt% CoBP for H_2 production.

Furthermore, to confirm that the photocatalytic activity of H_2 evolution is dependent on light absorption of a catalyst, the apparent quantum yield (AQY) of H_2 evolution of C_3N_4/5 wt% CoBP was measured under the same reaction conditions but different levels of monochromatic light irradiation (λ ± 5 nm for 420, 450, 500, 550 and 600 nm). The AQYs varied inversely with the UV–vis absorption spectrum of C_3N_4/5 wt% CoBP composite photocatalyst (Fig. 6b). Notably, the harvested visible photons dominated the driving force for the photocatalytic H_2 evolution reactions.[6] Interestingly, our C_3N_4/CoBP composite photocatalyst exhibited AQY of approximately 5.42% at 420 nm, which was higher than the AQYs other g-C_3N_4-based heterostructure photocatalysts (Table S2)[6,32,33].

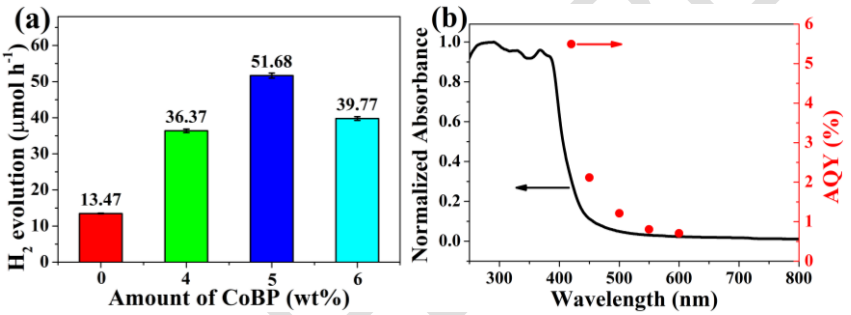

Fig. 6. (a)Comparison of the photocatalytic activity of C_3N_4/CoBP catalysts with different weight of CoBP, 1 wt% Pt as cocatalyst. (b) Wavelength-dependent apparent quantum yield (AQY) relationship for the photocatalytic hydrogen evolution.

Apart from the photocatalytic performance of H_2 evolution, an ideal photocatalyst must have photocatalytic stability and can be recycled for large-scale practical applications. To investigate photocatalytic stability, the C_3N_4/5 wt% CoBP composite photocatalyst was subjected to a recycling test involving five consecutive cycles of photocatalytic activity of H_2 evolution under the same experimental conditions (Fig. 7). No obvious loss of H_2 evolution activity was observed in the C_3N_4/5 wt% CoBP sample after 20 h of illumination, and the amount of H_2 evolved was nearly the same as that of the first cycle, implying that the composite photocatalyst exhibited good stability for photocatalytic H_2 production under prolonged visible-light irradiation. The XRD patterns of the C_3N_4/5 wt% CoBP composite photocatalyst before and after the recycling tests are shown in Fig. S7. No obvious change was observed in the C_3N_4/5 wt% CoBP composite before and after recycling. Overall, the findings of this study indicated the stability of the C_3N_4/5 wt% CoBP composite photocatalyst during the photocatalytic H_2 evolution. Therefore, the composite can be reused in photocatalytic reactions.

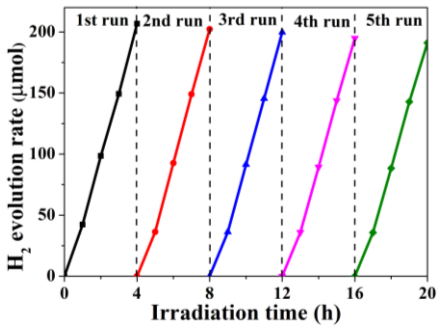

Fig.7. The reusability tests of C_3N_4/5 wt% CoBP with 1 % Pt cocatalyst for photocatalytic hydrogen production. Reaction conditions: 50 mg of photocatalyst, solvent [100 mL, H_2O/TEOA = 9:1 (vol/vol)] and a 300 W Xenon lamp as light source equipped with a cut-off filter (λ ≥ 420 nm), at 10 °C, and H_2 produced was evacuated after every 4 h.

The results demonstrated that CoBP plays a crucial role in the separation and migration of electron–hole pairs in C_3N_4/CoBP hybrid photocatalysts. This role benefits from the formation of a heterojunction between amorphous CoBP molecule and g-C_3N_4 nanosheet photocatalyst. The CB and VB energy levels of g-C_3N_4 are −1.12 and +1.57 eV (vs. NHE), respectively[35–37]. The CB and VB of CoBP were estimated using valence band X-ray photoelectron spectroscopy (VB-XPS) and UV–vis diffuse reflection spectra. As displayed in Fig. S8, the VB edge position of CoBP was 0.89 eV, and the CB was −0.7 eV. These findings suggested a possible mechanism for visible-light-induced H_2 production activity in the C_3N_4/CoBP composite (Fig. 8). The CB edge position of g-C_3N_4 was more negative than that of CoBP, and thus CoBP acted as an outstanding electron sink. These electrons were then transported to Pt nanoparticle to prolong the lifetime of charge carriers (Fig. 8). The remaining holes in the VB of g-C_3N_4 and CoBP were consumed by the sacrificial electron donor (TEOA; Fig. 8). Overall, CoBP served as a charge-separation centre that restrained the recombination of photogenerated electrons and holes in g-C_3N_4 and significantly improved the photocatalytic activity for H_2 production.

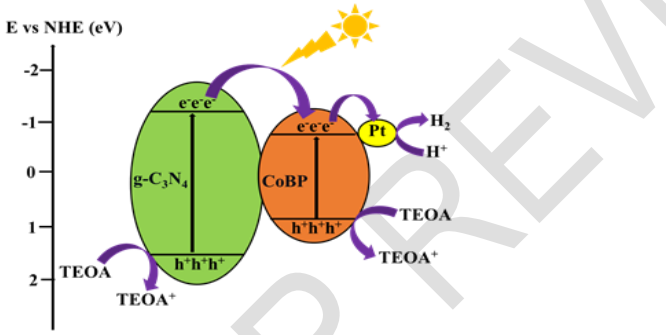

Fig. 8. Proposed mechanism of electron–hole transport process and photocatalytic activity of C_3N_4/CoBP heterostructure photocatalyst under visible-light irradiation.

4. CONCLUSION

We successfully fabricated a novel type of C_3N_4/CoBP composite photocatalyst by decorating CoBP on the surface of g-C_3N_4 through ultrasonication. The formation of a heterojunction between g-C_3N_4 and CoBP facilitated the migration and separation of photogenerated charge carriers in the system. Therefore, the C_3N_4/CoBP hybrid photocatalyst exhibited a higher level of photocatalytic activity for H_2 evolution than pure g-C_3N_4 under visible-light irradiation (λ ≥ 420 nm). Excellent charge transfer and separation led to a dramatic improvement in H_2 evolution rate, which reached up to 51.60 μmol h^{-1} under 5 wt% CoBP. This rate was 3.8 times that of bare g-C_3N_4 (13.47 μmol h^{-1}) and corresponded to an AQY of 5.42 % at 420 nm. Notably, the C_3N_4/CoBP composite photocatalyst displayed excellent photocatalytic stability and reusability for H_2 evolution after 20 h of irradiation. The CoBP is a promising material that combines with the low-cost g-C_3N_4 to form a C_3N_4/CoBP hybrid for practical use in photocatalytic H_2 production. In conclusion, this work offers a simple method for designing and developing not only highly efficient but also stable heterostructured photocatalysts for solar-to-chemical energy conversion.

REFERENCES

[1] Prasad C, Tang H, Liu Q, Bahadur I, Karlapudi S, Jiang Y. A latest overview on photocatalytic application of g-C_3N_4 based nanostructured materials for hydrogen production. International Journal of Hydrogen Energy 2020;45:337–79. https://doi.org/10.1016/j.ijhydene.2019.07.070.

[2] Yuan H, Fang F, Dong J, Xia W, Zeng X, Shangguan W. Enhanced photocatalytic hydrogen production based on laminated MoS_2/g-C_3N_4 photocatalysts. Colloids and Surfaces A: Physicochemical and Engineering Aspects 2022;641:128575. https://doi.org/10.1016/j.colsurfa.2022.128575.

[3] Fujishima A and Honda K. TIL. Nature 1972; 238: 37-38.

[4] Tahir W, Cheang TY, Li JH, Ling C, Lu XJ, Ullah I, et al. Interfacial Ti ≡ N bonding of a g-C_3N_4/$TiH_{1.92}$ type-II heterojunction photocatalyst significantly enhanced photocatalytic hydrogen evolution from water splitting. Catalysis Science and Technology 2022;12:2023–9. https://doi.org/10.1039/d1cy02039k.

[5] Kombo M, Chong HB, Ma LB, Sahar S, Fang XX, Zhao T, et al. Graphitic Carbon Nitride Decorated with Nickel(II)-

(3-Pyridyl) Benzimidazole Complexes and Pt Nanoparticles as a Cocatalyst for Photocatalytic Hydrogen Production from Water Splitting. ACS Applied Nano Materials 2020;3:10659–67. https://doi.org/10.1021/acsanm.0c01872.

[6] Kombo M, Ma LB, Liu YN, Fang XX, Ullah N, Odda AH, et al. Graphitic carbon nitride/CoTPP type-II heterostructures with significantly enhanced photocatalytic hydrogen evolution. Catalysis Science and Technology 2019;9:2196–202. https://doi.org/10.1039/c9cy00140a.

[7] Wang R, Ye C, Wang H, Jiang F. Z-Scheme $LaCoO_3$/g-$C_3N_4$for Efficient Full-Spectrum Light-Simulated Solar Photocatalytic Hydrogen Generation. ACS Omega 2020;5:30373–82. https://doi.org/10.1021/acsomega.0c03318.

[8] Jiang L, Wang K, Wu X, Zhang G, Yin S. Amorphous Bimetallic Cobalt Nickel Sul fi de Cocatalysts for Signi fi cantly Boosting Photocatalytic Hydrogen Evolution Performance of Graphitic Carbon Nitride : Efficient Interfacial Charge Transfer. ACS Applied Materials & Interfaces 2019;11:26898–908. https://doi.org/10.1021/acsami.9b07311.

[9] Chen S, Shen S, Liu G, Qi Y, Zhang F, Li C. Interface engineering of a CoOx/Ta_3N_5photocatalyst for unprecedented water oxidation performance under visible-light- Irradiation. Angewandte Chemie - International Edition 2015;54:3047–51. https://doi.org/10.1002/anie.201409906.

[10] Bai Y, Li C, Liu L, Yamaguchi Y, Bahri M, Yang H, et al. Photocatalytic Overall Water Splitting Under Visible Light Enabled by a Particulate Conjugated Polymer Loaded with Palladium and Iridium ** Angewandte 2022. https://doi.org/10.1002/ange.202201299.

[11] Novoa-cid M, Melillo A, Alvaro M, Baldovi HG. Photocatalytic Water Splitting Promoted by 2D and 3D Porphyrin Covalent Organic Polymers Synthesized by Suzuki-Miyaura Carbon-Carbon Coupling 2022.

[12] Wang X, Maeda K, Thomas A, Takanabe K, Xin G, Carlsson JM, et al. A metal-free polymeric photocatalyst for hydrogen production from water under visible light. Nature Materials 2009;8:76–80. https://doi.org/10.1038/nmat2317.

[13] Tahir W, Ullah S, Ullah I, Li JH, Ling C, Lu XJ, et al. Metallic WN plasmonic fabricated g-C_3N_4 significantly steered photocatalytic hydrogen evolution under visible and near-infrared light. Catalysis Science and Technology 2022;12:7369–78. https://doi.org/10.1039/d2cy01499h.

[14] Fang XX, Ma LB, Liang K, Zhao SJ, Jiang YF, Ling C, et al. The doping of phosphorus atoms into graphitic carbon nitride for highly enhanced photocatalytic hydrogen evolution. Journal of Materials Chemistry A 2019;7:11506–12. https://doi.org/10.1039/c9ta01646e.

[15] Zhao N, Kong L, Dong Y, Wang G, Wu X, Jiang P. Insight into the Crucial Factors for Photochemical Deposition of Cobalt Cocatalysts on g-C_3N_4Photocatalysts. ACS Applied Materials and Interfaces 2018;10:9522–31. https://doi.org/10.1021/acsami.8b01590.

[16] Hong Y, Li C, Li D, Fang Z, Luo B, Yan X, et al. Precisely tunable thickness of graphitic carbon nitride nanosheets for visible-light-driven photocatalytic hydrogen evolution. Nanoscale 2017;9:14103–10. https://doi.org/10.1039/c7nr05155g.

[17] Shalom M, Inal S, Fettkenhauer C, Neher D, Antonietti M. Improving carbon nitride photocatalysis by supramolecular preorganization of monomers. Journal of the American Chemical Society 2013;135:7118–21. https://doi.org/10.1021/ja402521s.

[18] Mao Z, Chen J, Yang Y, Wang D, Bie L, Fahlman BD. Novel g-C_3N_4/CoO Nanocomposites with Significantly Enhanced Visible-Light Photocatalytic Activity for H2 Evolution. ACS Applied Materials and Interfaces 2017;9:12427–35. https://doi.org/10.1021/acsami.7b00370.

[19] Jin Z, Wei T, Lixue Li, Li F, Tao R, Xu L. Loading Co_3N nanoparticles as efficient cocatalysts over $Zn_{0.5}Cd_{0.5}S$ for enhanced H_2 evolution under visible light. Dalton Transactions 2019;48:2676–82. https://doi.org/10.1039/c8dt05087b.

[20] Li Z, Wu Y, Lu G. Highly efficient hydrogen evolution over $Co(OH)_2$ nanoparticles modified g-C_3N_4 co-sensitized by Eosin Y and Rose Bengal under Visible Light Irradiation. Applied Catalysis B: Environmental 2016;188:56–64. https://doi.org/10.1016/j.apcatb.2016.01.057.

[21] Sun H, Xu X, Yan Z, Chen X, Jiao L, Cheng F, et al. Superhydrophilic amorphous Co-B-P nanosheet electrocatalysts with Pt-like activity and durability for the hydrogen evolution reaction. Journal of Materials Chemistry A 2018;6:22062–9. https://doi.org/10.1039/C8TA02999G.

[22] Chunduri A, Gupta S, Bapat O, Bhide A, Fernandes R, Patel MK, et al. A unique amorphous cobalt-phosphide-boride bifunctional electrocatalyst for enhanced alkaline water-splitting. Applied Catalysis B: Environmental 2019;259:118051. https://doi.org/10.1016/j.apcatb.2019.118051.

[23] Kim J, Kim H, Kim SK, Ahn SH. Electrodeposited amorphous Co-P-B ternary catalyst for hydrogen evolution reaction. Journal of Materials Chemistry A 2018;6:6282–8. https://doi.org/10.1039/c7ta11033b.

[24] Liu YN, Zhou X, Shen CC, Zhao ZW, Jiang YF, Ma LB, et al. Hydrogen-bonding-assisted charge transfer: Significantly enhanced photocatalytic H_2 evolution over g-C_3N_4 anchored with ferrocene-based hole relay. Catalysis Science and Technology 2018;8:2853–9. https://doi.org/10.1039/c8cy00488a.

[25] Wang W, Liu P, Wu K, Tan S, Li W, Yang Y. Preparation of hydrophobic reduced graphene oxide supported Ni-B-P-O and Co-B-P-O catalysts and their high hydrodeoxygenation activities. Green Chemistry 2016;18:984–8.

https://doi.org/10.1039/c5gc02073e.
[26] Men Y, Su J, Du X, Liang L, Cheng G, Luo W. CoBP nanoparticles supported on three-dimensional nitrogen-doped graphene hydrogel and their superior catalysis for hydrogen generation from hydrolysis of ammonia borane. Journal of Alloys and Compounds 2018;735:1271–6. https://doi.org/10.1016/j.jallcom.2017.11.137.
[27] Jia X, Sang Z, Sun L, Xu F, Pan H, Zhang C, et al. Graphene-Modified Co-B-P Catalysts for Hydrogen Generation from Sodium Borohydride Hydrolysis. Nanomaterials 2022;12:1–14. https://doi.org/10.3390/nano12162732.
[28] Yi SS, Yan JM, Wulan BR, Li SJ, Liu KH, Jiang Q. Noble-metal-free cobalt phosphide modified carbon nitride: An efficient photocatalyst for hydrogen generation. Applied Catalysis B: Environmental 2017;200:477–83. https://doi.org/10.1016/j.apcatb.2016.07.046.
[29] Ma LB, Liu YN, Liang K, Fang XX, Sahar S, Kombo M, et al. Hantzsch ester as hole relay significantly enhanced photocatalytic hydrogen production. Catalysis Science and Technology 2018;8:6123–8. https://doi.org/10.1039/c8cy01922c.
[30] Zhu X, Yu S, Gong X, Xue C. In Situ Decoration of $Zn_xCd_{1-x}S$ with FeP for Efficient Photocatalytic Generation of Hydrogen under Irradiation with Visible Light. ChemPlusChem 2018;83:825–30. https://doi.org/10.1002/cplu.201800316.
[31] Wang DH, Pan JN, Li HH, Liu JJ, Wang YB, Kang LT, et al. A pure organic heterostructure of μ-oxo dimeric iron(III) porphyrin and graphitic-$C_3N_4$for solar H_2 production from water. Journal of Materials Chemistry A 2015;4:290–6. https://doi.org/10.1039/c5ta07278f.
[32] Ye R, Fang H, Zheng YZ, Li N, Wang Y, Tao X. Fabrication of $CoTiO_3$/g-C_3N_4 Hybrid Photocatalysts with Enhanced H_2 Evolution: Z-Scheme Photocatalytic Mechanism Insight. ACS Applied Materials and Interfaces 2016;8:13879–89. https://doi.org/10.1021/acsami.6b01850.
[33] Chen J, Zhao D, Diao Z, Wang M, Shen S. Ferrites boosting photocatalytic hydrogen evolution over graphitic carbon nitride: a case study of (Co, Ni)Fe_2O_4 modification. Science Bulletin 2016;61:292–301. https://doi.org/10.1007/s11434-016-0995-0.
[34] Wang W, Liu S, Nie L, Cheng B, Yu J. Enhanced photocatalytic H_2-production activity of TiO_2 using $Ni(NO_3)_2$ as an additive. Physical Chemistry Chemical Physics 2013;15:12033–9. https://doi.org/10.1039/c2cp43628k.
[35] Obregón S, Colón G. Improved H_2 production of Pt-TiO_2/g-C_3N_4-MnO_x composites by an efficient handling of photogenerated charge pairs. Applied Catalysis B: Environmental 2014;144:775–82. https://doi.org/10.1016/j.apcatb.2013.07.034.
[36] Fu J, Chang B, Tian Y, Xi F, Dong X. Novel C_3N_4-CdS composite photocatalysts with organic-inorganic heterojunctions: In situ synthesis, exceptional activity, high stability and photocatalytic mechanism. Journal of Materials Chemistry A 2013;1:3083–90. https://doi.org/10.1039/c2ta00672c.
[37] Huang L, Xu H, Li Y, Li H, Cheng X, Xia J, et al. Visible-light-induced WO_3/g-C_3N_4 composites with enhanced photocatalytic activity. Dalton Transactions 2013;42:8606–16. https://doi.org/10.1039/c3dt00115f.

SUPPORTING INFORMATION

Fig. S1. Schematic illustration of the formation of amorphous CoBP sample.

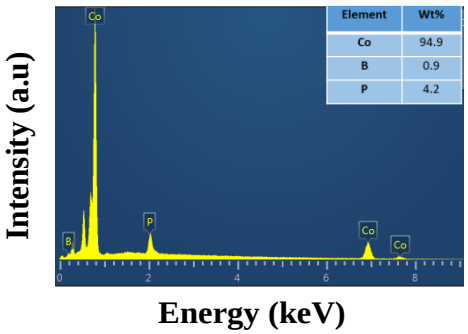

Fig. S2. High resolution XPS spectra of (a) Co 2p region. (b) P 2p region. (c) B 1s region for CoBP sample.

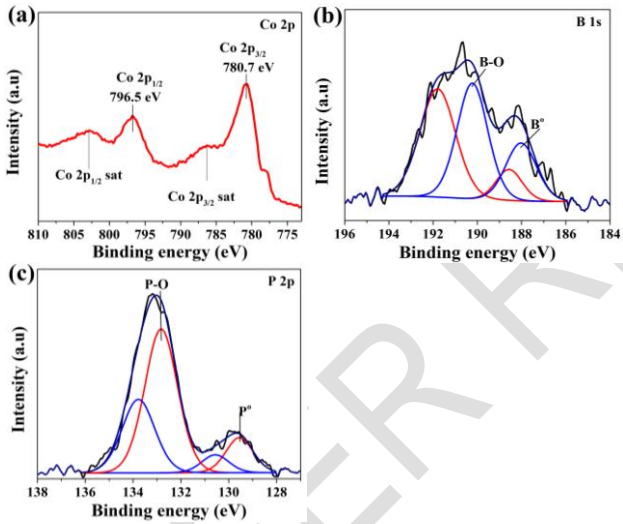

Fig. S3. High resolution XPS spectra of (a) Co 2p region. (b) P 2p region. (c) B 1s region for CoBP sample.

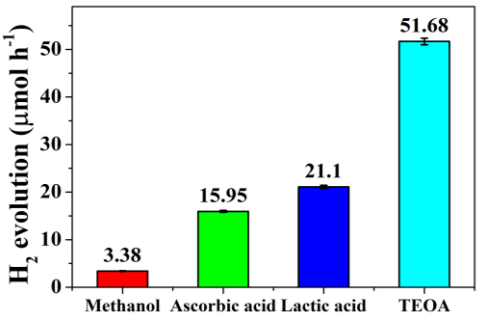

Fig. S4. Comparison of photocatalytic hydrogen evolution rates on C_3N_4/5 wt% CoBP composite photocatalyst in the presence of different sacrificial reagents under visible light (λ≥ 420 nm). Reaction conditions: Catalyst, 50 mg; 100 mL of solution containing sacrificial reagents; light source, xenon lamp (300 W) with a cutoff filter; temperature, 10 ºC.

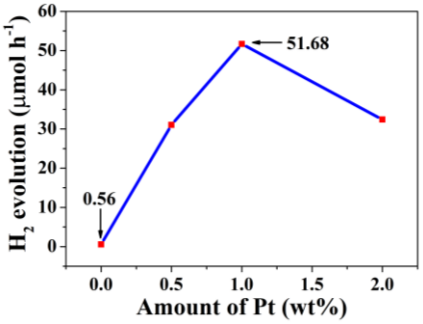

Fig. S5. Effect of the Pt loading amounts on photocatalytic hydrogen evolution of C_3N_4/5 wt% CoBP under visible light irradiation (λ ≥ 420 nm).

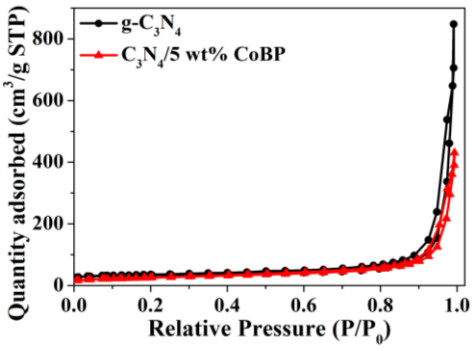

Fig. S6. Nitrogen adsorption-desorption isotherms of pure g-C_3N_4 and C_3N_4/5 wt% CoBP composite photocatalysts.

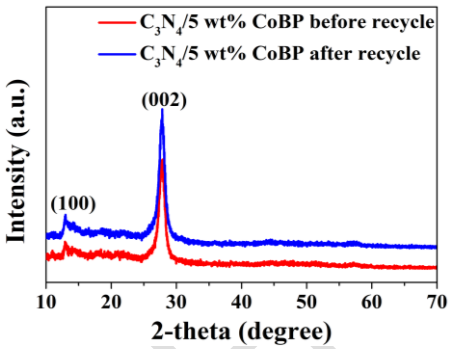

Fig. S7. XRD spectra of C_3N_4/5 wt% CoBP composite photocatalysts before and after recycle.

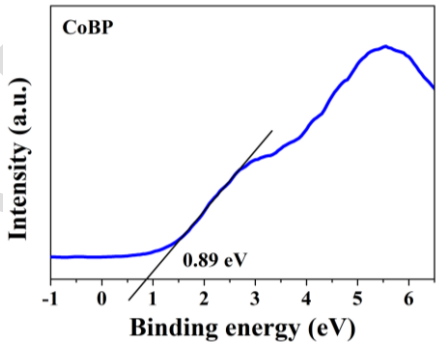

Fig. S8. Valence bandXPS spectra of CoBP sample.

Table S1. Fitting parameters of EIS results

Samples	Rs	Rct
g-C_3N_4 photocatalysts	25.67	686.1
C_3N_4/5 wt% CoBP composite photocatalysts	19.58	652.1

Table S2.Comparison of the hydrogen production activity and AQY value of various g-C_3N_4-based heterostructure photocatalysts reported previously.

Photocatalysts	Pt [wt%]	Light source	HER $\mu molh^{-1}g^{-1}$	AQY [%]	Refs.

g-C_3N_4/CoTPP	1	300 W Xe lamp (λ ≥ 420 nm)	938.6	4.2 (λ = 420 nm)	[1]
$CoTiO_3$/g-C_3N_4	3	300 W Xe lamp (under simulated solar light irradiation)	858	3.23 (λ = 420 nm)	[2]
g-C_3N_4/$CoFe_2O_4$	1	300 W Xe lamp (λ > 420 nm)	186.1	3.35 (λ = 420 nm)	[3]
g-C_3N_4/CoO	3	300 W Xe lamp (λ ≥ 400 nm)	651.3	NA	[4]
C_3N_4/CoBP	1	300 W Xe lamp (λ ≥ 420 nm)	1033.6	5.42 (λ = 420 nm)	Our work

REFERENCES

[1] Kombo M, Ma LB, Liu YN, Fang XX, Ullah N, Odda AH, et al. Graphitic carbon nitride/CoTPP type-II heterostructures with significantly enhanced photocatalytic hydrogen evolution. Catalysis Science and Technology 2019;9:2196–202. https://doi.org/10.1039/c9cy00140a.

[2] Ye R, Fang H, Zheng YZ, Li N, Wang Y, Tao X. Fabrication of $CoTiO_3$/g-C_3N_4 Hybrid Photocatalysts with Enhanced H_2 Evolution: Z-Scheme Photocatalytic Mechanism Insight. ACS Applied Materials and Interfaces 2016;8:13879–89. https://doi.org/10.1021/acsami.6b01850.

[3] Chen J, Zhao D, Diao Z, Wang M, Shen S. Ferrites boosting photocatalytic hydrogen evolution over graphitic carbon nitride: a case study of (Co, Ni)Fe_2O_4 modification. Science Bulletin 2016;61:292–301. https://doi.org/10.1007/s11434-016-0995-0.

[4] Mao Z, Chen J, Yang Y, Wang D, Bie L, Fahlman BD. Novel g-C_3N_4/CoO Nanocomposites with Significantly Enhanced Visible-Light Photocatalytic Activity for H_2 Evolution. ACS Applied Materials and Interfaces 2017;9:12427–35. https://doi.org/10.1021/acsami.7b00370.